



**Providing Choice & Value**  
Generic CT and MRI Contrast Agents

**FRESENIUS  
KABI**

**CONTACT REP**

**AJNR**

**Simultaneous Measurement of Regional  
Cerebral Blood Flow by Perfusion CT and  
Stable Xenon CT: A Validation Study**

Max Wintermark, Jean-Philippe Thiran, Philippe Maeder,  
Pierre Schnyder and Reto Meuli

This information is current as  
of July 16, 2025.

*AJNR Am J Neuroradiol* 2001, 22 (5) 905-914  
<http://www.ajnr.org/content/22/5/905>

# Simultaneous Measurement of Regional Cerebral Blood Flow by Perfusion CT and Stable Xenon CT: A Validation Study

Max Wintermark, Jean-Philippe Thiran, Philippe Maeder, Pierre Schnyder, and Reto Meuli

**BACKGROUND AND PURPOSE:** Knowledge of cerebral blood flow (CBF) alterations in cases of acute stroke could be valuable in the early management of these cases. Among imaging techniques affording evaluation of cerebral perfusion, perfusion CT studies involve sequential acquisition of cerebral CT sections obtained in an axial mode during the IV administration of iodinated contrast material. They are thus very easy to perform in emergency settings. Perfusion CT values of CBF have proved to be accurate in animals, and perfusion CT affords plausible values in humans. The purpose of this study was to validate perfusion CT studies of CBF by comparison with the results provided by stable xenon CT, which have been reported to be accurate, and to evaluate acquisition and processing modalities of CT data, notably the possible deconvolution methods and the selection of the reference artery.

**METHODS:** Twelve stable xenon CT and perfusion CT cerebral examinations were performed within an interval of a few minutes in patients with various cerebrovascular diseases. CBF maps were obtained from perfusion CT data by deconvolution using singular value decomposition and least mean square methods. The CBF were compared with the stable xenon CT results in multiple regions of interest through linear regression analysis and bilateral *t* tests for matched variables.

**RESULTS:** Linear regression analysis showed good correlation between perfusion CT and stable xenon CT CBF values (singular value decomposition method:  $R^2 = 0.79$ , slope = 0.87; least mean square method:  $R^2 = 0.67$ , slope = 0.83). Bilateral *t* tests for matched variables did not identify a significant difference between the two imaging methods ( $P > .1$ ). Both deconvolution methods were equivalent ( $P > .1$ ). The choice of the reference artery is a major concern and has a strong influence on the final perfusion CT CBF map.

**CONCLUSION:** Perfusion CT studies of CBF achieved with adequate acquisition parameters and processing lead to accurate and reliable results.

Viability of the cerebral parenchyma is dependent on cerebral blood flow (CBF) (1, 2). Complex autoregulation processes ensure the adjustment of regional CBF to local energetic needs, determined by the activity level of local neurons (3, 4). CBF alterations are encountered in association with a variety of pathologic conditions, the most frequent

being strokes. Strokes affect 500,000 patients in the United States every year (5). Cerebral infarcts occur when CBF values are  $<10$  to  $15 \text{ cc}/[100 \text{ g} \times \text{min}]$ , whereas penumbra, relating to reversible cerebral ischemia, happens with CBF between 15 and  $20 \text{ cc}/[100 \text{ g} \times \text{min}]$  (6–8). Present indications for a thrombolytic therapy rely on the time interval between the beginning of symptoms (inferior or superior to 3 hr) and the native cerebral CT findings (5, 9, 10). Knowledge of a quantitative map of CBF, indicating the severity and potential reversibility of neuronal damages, would perhaps allow for the clinical use of the theoretical thresholds mentioned above; thrombolysis achieved when the penumbra prevails over the infarcted area might not only be more profitable but furthermore might decrease the risk of intracranial bleeding (11, 12).

Different imaging techniques are now available to evaluate CBF, notably stable xenon CT and perfusion CT studies. Stable xenon CT relates to dy-

Received August 31, 2000; accepted after revision December 11.

From the Department of Diagnostic and Interventional Radiology (M.W., R.M., P.S., P.M.), University Hospital, and the Signal Processing Laboratory (J.-P.T.), Swiss Federal Institute of Technology, Lausanne, Switzerland.

This work was accepted as an oral presentation at the 86th Scientific Assembly and Annual Meeting of the Radiological Society of North America, Chicago, 2000.

Address reprint requests to Reto Meuli, Associate Professor, Department of Diagnostic and Interventional Radiology, University Hospital, CHUV—BH10, 1011 Lausanne, Switzerland.

© American Society of Neuroradiology

namic CT scanning during inhalation by the patient of a gas mixture containing stable xenon and oxygen. Alveolar xenon accumulation is measured end-tidally by a thermoconductivity analyzer and assumed to be equal to arterial xenon concentration. Stable xenon is a diffusible gas that progressively pervades cerebral blood and neurons on a well-balanced basis. Its radiopacity relates cerebral increase of CT units on successive cerebral CT sections to an increase of the parenchymal concentration of stable xenon. Stable xenon CT data analysis is realized through applying the equilibrating indicator model (13–20), which relies on the Fick principle:

$$\frac{dQ(t)}{dt} = \text{CBF} \cdot (C_a(t) - C_v(t)) \quad (1)$$

where  $C_a(t)$  and  $C_v(t)$  designate the instantaneous arterial and venous concentration of the indicator at time  $t$ , whereas  $Q(t)$  designates the amount of indicator in the local vascular networks in connection with time  $t$ . The equilibrating indicator model supposes a balance between the venous,  $C_v(t)$ , and the parenchymal,  $C_b(t)$ , concentrations of the indicator:

$$C_b(t) = \lambda * C_v(t) \quad (2)$$

where  $\lambda$  relates to the cerebral parenchyma-blood partition coefficient of the indicator. Combination and development of equations 1 and 2 result in the supporting equation of the equilibrating indicator model:

$$C_b(T) = \lambda \cdot K \cdot \int_{t=0}^T C_a(t) \cdot e^{-K \cdot (T-t)} \cdot dt \quad (3)$$

with

$$K = \frac{\text{CBF}}{\lambda} \quad (4)$$

The CBF map inferred from stable xenon CT data analysis has been compared with that provided by radiolabeled microsphere studies and thus proved quantitative and accurate (21–23).

Stable xenon CT, however, necessitates excellent collaboration from the patient, as well as specialized and expensive equipment. It may occasionally be responsible for a decrease in the respiratory rate (yet without reported respiratory failure), headaches, nausea, vomiting, and convulsions. In a large study involving 1839 patients, these side effects were observed, respectively, in 3.6%, 0.4%, 0.2%, and 0.2% of the patients (24).

Perfusion CT studies involve sequential acquisition of cerebral CT sections achieved on an axial mode, during the IV administration of iodinated contrast material. Perfusion CT data consist of contrast enhancement profiles obtained at each pixel, the latter relating linearly to the time-concentration curves of the contrast material. Analysis of these curves is realized according to the central volume

principle, which has been reported to lead to the most accurate results (25–31). The regional cerebral blood volume map is inferred from a quantitative estimation of the partial volume averaging effect, completely absent in a reference pixel at the center of the large superior sagittal venous sinus:

$$\text{CBV} = \frac{\text{area under the curve in a parenchymal pixel}}{\text{area under the curve in the reference pixel}} \quad (5)$$

where CBV stands for cerebral blood volume with a correction factor to take into consideration that iodinated contrast material is restricted to the plasma phase of the blood (31–36). The impulse function and the related mean transit time maps result from a deconvolution of the parenchymal time-concentration curves by a reference arterial curve. Finally, combination of cerebral blood volume and mean transit time at each pixel leads to a CBF value (Fig 1) through the simple equation (29–31):

$$\text{CBF} = \frac{\text{CBV}}{\text{MTT}} \quad (6)$$

where MTT stands for mean transit time. Perfusion CT studies are easy to perform at all institutions with a CT unit, even for acutely affected patients. When achieved with a multi-detector CT unit, allow for examination of two 10-mm cerebral CT sections. The study is quick and does not necessitate extra material or specialized technicians. They are not time-consuming, because they can readily complete the cerebral CT survey undergone by every stroke patient (37).

Perfusion CT values of CBF have proved to be accurate in animals (38, 39) and afford plausible values in humans (37). However, they have never been validated against another CBF imaging technique in humans or have been so only in a limited fashion (40).

## Methods

Nine patients who had to undergo a stable xenon CT to assess brain perfusion were prospectively identified during the period from September 1999 to May 2000 and were included in the study. Classical contraindications regarding the IV administration of iodinated contrast material were respected. The reasons for brain perfusion evaluation in of patients are shown in Table 1. For these patients, perfusion CT examinations were performed within a few minutes after the end of the stable xenon CT. Three patients underwent both stable xenon CT and perfusion CT studies twice: patients 2 and 3, 3 months after the first xenon CT perfusion CT couple; patient 3, 4 months later. In patients 3, 4, 5, and 6, the cerebral vascular reserve was evaluated by performing two stable xenon CT examinations at a 20-min interval, before and after the IV administration of 1 g acetazolamide. For these patients, the perfusion CT was performed immediately after the second stable xenon CT. This study protocol was approved by our hospital ethics committee, and informed consent was obtained from each patient before the perfusion CT was performed.

Stable xenon CT studies were performed on a CT unit equipped with a multi-detector array (Lightspeed CT Unit; General Electric, Milwaukee, WI). The imaging protocol con-

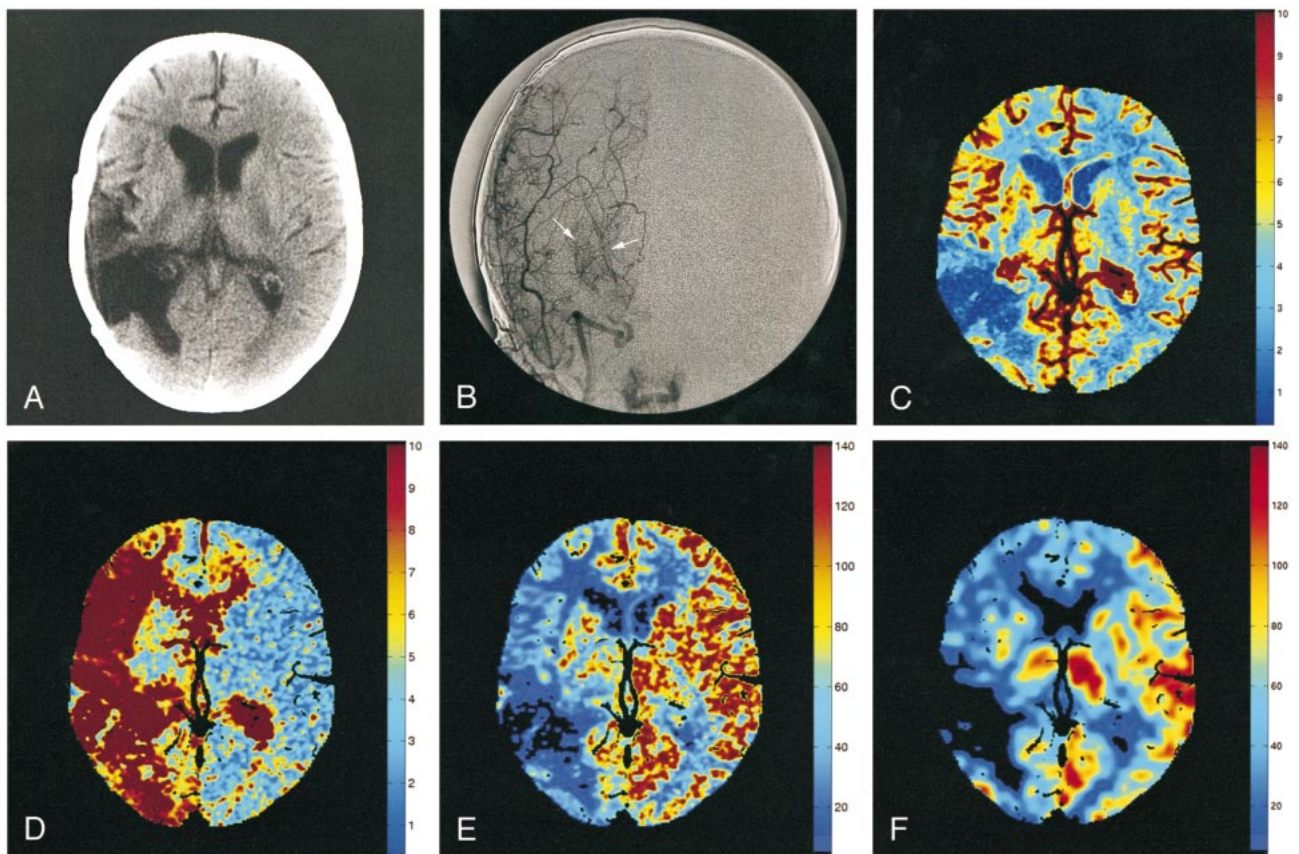


FIG 1. Images from the case of a 53-year-old woman with Moya Moya syndrome.

A, Ten-millimeter cerebral CT section shows encephalomalacia at the site of an excised right temporoparietal arteriovenous malformation.

B, Anteroposterior angiographic view displays Moya networks (arrows) due to the occlusion of the right MCA.

C, Perfusion CT studies led to a regional cerebral blood volume map (cc/100 g), resulting from a quantitative estimation of the partial volume averaging effect at each pixel. The cerebral blood volume map is normal, except in the resected area.

D, Mean transit time map inferred from a deconvolution operation. The mean transit time is abnormally prolonged in the right cerebral hemisphere.

E, Regional CBF map (cc/[100 g  $\times$  min]), with the CBF at each pixel resulting from division of cerebral blood volume by relating mean transit time. CBF is abnormally lowered ipsilaterally, especially in the resected area.

F, Corresponding stable xenon CT scan is closely related to the CBF map shown in panel E.

TABLE 1: Characteristics of patients undergoing both stable xenon CT and perfusion CT studies of regional CBF

Patient (No)/Age [y]/Sex	Diagnosis	Rationale For Brain Perfusion Imaging	Location of Lowered CBF (ROI)
1/53/M	Subarachnoid hemorrhage	Brain ischemia symptomatology during follow-up	No pathological area
2/57/F	Left internal carotid giant aneurysm	VIIIth cranial nerve compression symptomatology	Left MCA territory
3/53/F	Moya Moya syndrome	Partial left facio-brachial hemisyndrome	Moya networks neighbouring area
4/39/M	Moya Moya syndrome	Repeated faintness episodes without loss of consciousness	Moya networks neighbouring area
5/58/M	Atherosclerotic left internal carotid occlusion	Transitory ischemic accidents following extra-intracranial bypass	Left hemisphere, especially left temporo-parietal infarct
6/60/M	Left subclavian steal syndrome	Estimation of the cerebral vascular reserve	Left hemisphere
7/50/F	Herpetic cerebral vasculitis	Right facio-brachio crural hemisyndrome	Left lenticular cerebral infarct
8/56/F	Subarachnoid hemorrhage	Brain ischemia symptomatology during follow-up	Bilateral ACA and MCA territories
9/31/M	Rasmussen encephalitis	Spastic tetraparesia and myoclonic epilepsy	Left hemisphere



**TABLE 2: Overview of cerebral parenchymal CBF values (average values  $\pm$  standard deviation) obtained from stable xenon CT and perfusion CT studies with single value deconvolution (SVD) and least mean square deconvolution (LMS) methods**

CBF [cc/(100 g $\times$ min)]	Stable Xenon CT Values of CBF	SVD Perfusion CT Values of CBF	LMS Perfusion CT Values of CBF
Healthy parenchyma without ACA and MCA branches	49 $\pm$ 25	46 $\pm$ 24	47 $\pm$ 26
Gray matter	71 $\pm$ 15	68 $\pm$ 13	69 $\pm$ 17
White matter	28 $\pm$ 10	26 $\pm$ 10	25 $\pm$ 9
Healthy parenchyma with ACA and MCA branches	54 $\pm$ 27 (*)	70 $\pm$ 14 (*)	100 $\pm$ 23 (*)
Pathological parenchyma	14 $\pm$ 9	14 $\pm$ 10	15 $\pm$ 11

\* Statistically significant differences could be observed only between CBF values indicated by an asterisk.

sisted of six contiguous 10-mm sections (80 kVp, 240 mAs) located on the cerebral hemispheres. This protocol was repeated two times before and four times during an inhalation of a gas mixture containing 28% stable xenon, 25% oxygen, and 47% air, to a total of 6 min. The obtained data were analyzed on a PC unit with dedicated post-processing software (XeCT System 2; Diversified Diagnostic Products Inc, Houston, TX).

For the perfusion CT study, two adjacent levels among the six examined ones were selected at the level of the basal nuclei. Twenty-five successive 10-mm CT sections were obtained every 2 s at these two adjacent levels (multi-detector array CT unit), with a total acquisition time of 50 s. Acquisition parameters were 80 kVp and 200 mAs. CT was initiated 2 s before the IV administration of 1.3 cc/kg of iohexol by means of a power injector at a rate of 5 cc/s. The delay before injection of the contrast material allowed for the acquisition of baseline images without contrast enhancement. The sedation conditions were the same for perfusion CT and stable xenon CT if such sedation was used (patient 8). Finally, acquisition of perfusion CT data began 3 min after the end of the stable xenon CT study, allowing a complete wash-out of the stable xenon from the expired air and from the brain, as shown by the thermconductivity measurements of end-tidal stable xenon concentrations.

This perfusion CT protocol involved an additional radiation dose of 291 mSv. Regarding the stochastic effects of radiations, this dose, once redistributed on the entire cerebral volume, amounted to 29 mSv, which is inferior to the dose of a standard cerebral CT examination (40–60 mSv) (see Appendix).

Stable xenon CT results and perfusion CT data were transferred to a workstation for computer processing and comparison. Perfusion CT data were analyzed by both the CT perfusion software working on an Advantage Window workstation (GE Medical Systems, Milwaukee, WI) and a software that we develop, which will soon be available as freeware on the web. Both systems rely on the central volume principle (31) and basically intend to solve the overdetermined set of equations corresponding to the algebraic formulation of the deconvolution of parenchymal time-concentration curves by a reference arterial curve. They use two different deconvolution methods: the singular value decomposition (SVD) and the conventional least mean square (LMS) methods (see Appendix). In both cases, the reference artery was automatically selected by the software (thus avoiding interobserver variability) as the pixel with the shorter time to peak on the corresponding time-concentration curve in the area drawn by the observer, either around the anterior cerebral artery (ACA) or around the middle cerebral artery (MCA).

Final results included three CBF maps: a stable xenon CT map, a perfusion CT map obtained by SVD, and a perfusion CT map obtained by LMS. These were obtained for each of the two examined levels that underwent CT during the 12 examinations of the nine patients. By using a mouse-guided cursor, freehand regions of interest (ROI) were drawn identically on the three sets of CBF maps to conduct comparisons (ap-

proximately 30 ROI for each section level in every patient). ROI were obtained in healthy cerebral areas without ACA and MCA branches (approximately 10 ROI), in healthy cerebral areas with ACA and MCA branches (approximately 10 ROI), and in pathologically abnormal cerebral areas (approximately 10 ROI). An average value was then calculated for each ROI type at each section level in every patient. All the ROI were drawn by the same reader and then checked by a second reader to warrant their adequate choice regarding location. When there was doubt regarding the location of an ROI, that ROI was suppressed and replaced by another one chosen by both readers. Statistical analysis was conducted on CBF values associated with the various ROI. Bilateral *t* tests for matched variables were used to compare CBF values, and linear regression analysis was used to evaluate the correlation of data sets. Significance was stated at  $P < .001$ .

## Results

Perfusion CT studies were performed with no complications for all nine patients, whereas stable xenon CT examinations were responsible for a decrease in respiratory rate in one patient (patient 5) and for hallucinations in another (patient 3). Stable xenon CT studies were, in all cases, of excellent quality, with confidence rates superior to 95%; these confidence rates estimated the obtained data confidence and, more precisely, the quality of the fitting of the enhancement curves in the cerebral pixels consecutive to xenon diffusion. The measured values of CBF are summarized in Table 2, and the results of the comparison between perfusion CT (Fig 2B and C) and stable xenon CT (Fig 2A) are displayed in Figure 3.

In healthy cerebral regions without ACA and MCA branches, there was an excellent correlation between CBF maps resulting from stable xenon CT and perfusion CT studies. Linear regression analysis revealed an overall strong correlation between stable xenon CT and SVD perfusion CT maps of CBF ( $CBF_{SVD} = 4 + 0.87 \times CBF_{Xe}$ ,  $R^2 = 0.79$ ), and between stable xenon CT and LMS perfusion CT maps of CBF ( $CBF_{LMS} = 6 + 0.83 \times CBF_{Xe}$ ,  $R^2 = 0.67$ ). Bilateral *t* tests for matched variables showed that none of the observed differences were statistically significant ( $P = .17$  for SVD xenon and 0.19 for LMS xenon). Both deconvolution methods were equivalent ( $CBF_{LMS} = 5 + 0.90 \times CBF_{SVD}$ ,  $R^2 = 0.72$ ), with the *P* value for the corresponding *t* test being 0.89.

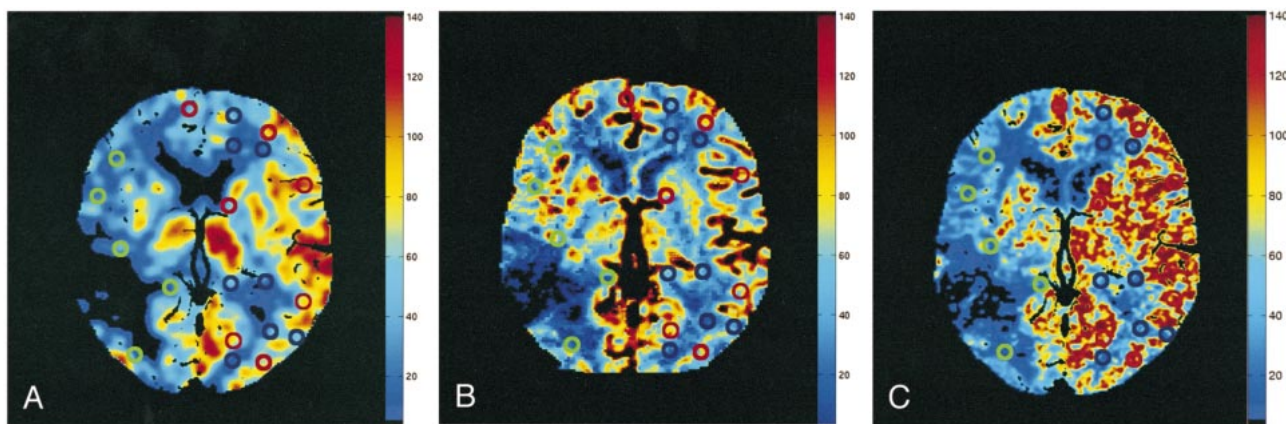


FIG 2. CBF maps of the same patient shown in Figure 1 show perfusion CT studies of CBF ( $\text{cc}/[100 \text{ g} \times \text{min}]$ ). The three CBF maps agree and show a 20% decrease in the left CBF. Cerebral regions with normal (*blue ROI*) and lowered (*green ROI*) CBF values are adequately displayed on the three CBF maps. With the LMS perfusion CT software, pixels with ACA and MCA branches (*red ROI*) show discretely increased CBF values, whereas they are filtered away with the SVD perfusion CT software. SVD and LMS perfusion CT software differ regarding the detection thresholds of vessels and spatial filtering for the final display.

A, Stable xenon CT scan.

B, SVD method.

C, LMS method.

In healthy cerebral regions with ACA and MCA branches, perfusion CT studies showed a significant ( $P < .001$  in the related  $t$  test) trend to exceed CBF values compared with those of stable xenon CT ( $\text{CBF}_{\text{SVD}} = 62 + 0.15 \times \text{CBF}_{\text{Xe}}$ ,  $R^2 = 0.44$ ;  $\text{CBF}_{\text{LMS}} = 77 + 0.42 \times \text{CBF}_{\text{Xe}}$ ,  $R^2 = 0.35$ ).

In pathologically abnormal cerebral regions, an overall decrease in CBF was noticed, with average values amounting to approximately  $15 \text{ cc}/100 \text{ g} \times \text{min}$ . An excellent correlation was shown between perfusion CT and stable xenon CT studies or CBF ( $\text{CBF}_{\text{SVD}} = 3 + 0.84 \times \text{CBF}_{\text{Xe}}$ ,  $R^2 = 0.58$ ;  $\text{CBF}_{\text{LMS}} = 4 + 0.85 \times \text{CBF}_{\text{Xe}}$ ,  $R^2 = 0.43$ ), with a  $P$  value for the corresponding  $t$  tests equal to 0.26 for SVD xenon and 0.31 for LMS xenon. Both deconvolution methods lead to similar results ( $\text{CBF}_{\text{LMS}} = 2 + 0.93 \times \text{CBF}_{\text{SVD}}$ ,  $R^2 = 0.69$ ).

### Discussion

Stable xenon CT relies on the equilibrating indicator model, which indicates that the balance of concentrations of a diffusible indicator between blood and cerebral parenchyma is more or less rapidly realized in the various cerebral areas, according to the importance of the corresponding local CBF. Knowledge of the blood (or alveolar) and parenchymal concentration curves leads to the balance rates and to the CBF values for each pixel (13–20).

On the other hand, perfusion CT data analysis is realized through the central volume principle (25–36). The latter describes the behavior of an iodinated contrast material bolus crossing the cerebral capillary networks, with subsequent modifications of contrast enhancement profiles. Iodinated contrast material is limited to blood vessels, at least at first pass and in healthy cerebral parenchyma.

Perfusion CT studies of CBF are not time-consuming and are well tolerated. They verify classical contraindications regarding the IV administration of iodinated contrast material. On the other hand, the IV administration of nonionic iodinated contrast material can reasonably be achieved even in patients who have suffered acute stroke (41).

Perfusion CT studies do not require any special equipment, except for dedicated post-processing software, which will soon be available as freeware on the Internet.

Even with a multi-detector CT unit, perfusion CT coverage of the brain is inferior to that of stable xenon CT, because only two 10-mm cerebral CT sections can be examined. This is mainly because of the much quicker kinetics of iodinated contrast material compared with that of stable xenon CT. However, the purpose of our study was to compare the corresponding sections in perfusion CT and stable xenon CT and not brain coverage.

Validity of perfusion CT results has been shown in animal studies (38, 39), whereas results in human studies have been shown only to correlate with the values reported in the literature (37). In 12 examinations involving nine patients, we experimentally showed that perfusion CT values of CBF have excellent correlation with those of stable xenon CT, the latter being a brain perfusion imaging technique that has proved accurate (21–23). More precisely, linear regression analysis in healthy cerebral regions without ACA and MCA branches showed a slope close to unity and correlation coefficients ( $R^2$ ) superior to 0.65. Because both examinations were performed within a few minutes of each other, it can be assumed that no CBF modification occurred in between and that our study was thus not biased.

Perfusion CT values of CBF estimated in pixels that include not only cerebral parenchyma but also

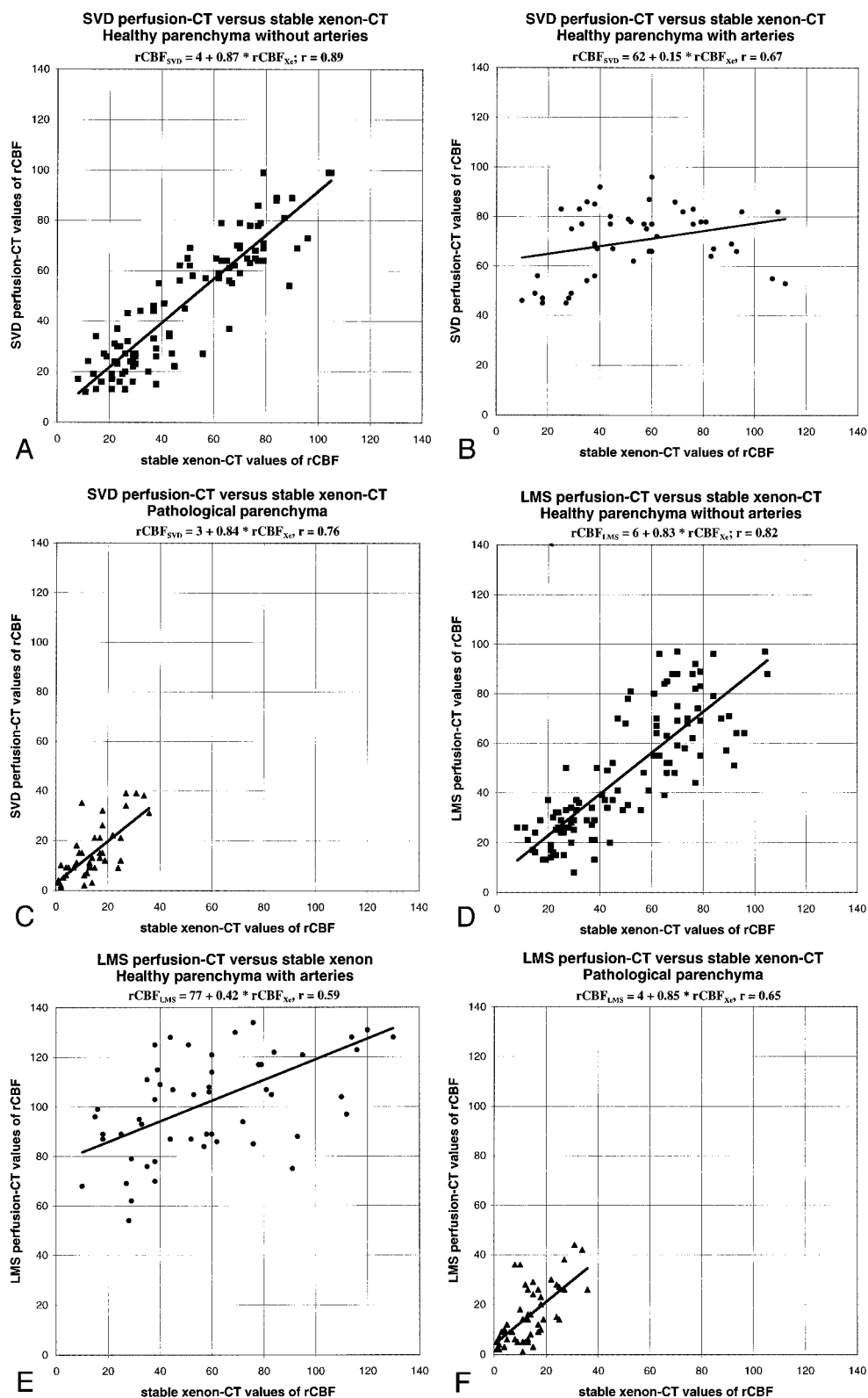


FIG 3. Scatter plots between stable xenon CT and SVD or LMS deconvolution perfusion CT values of CBF ( $cc/[100\text{ g} \times \text{min}]$ ).

A, Image obtained using the SVD method. Healthy cerebral regions without ACA and MCA branches show linear regression with strong correlation and slopes close to unity.

B, Image obtained using the SVD method. In healthy cerebral regions with ACA and MCA branches, perfusion CT values of CBF tend to exceed stable xenon CT values.

C, Image obtained using the SVD method. Pathologically abnormal cerebral regions show linear regression with strong correlation and slopes close to unity.

ACA and MCA branches significantly exceed stable xenon CT values. Because the CBF map should ideally display only capillary blood flow, perfusion CT values estimated in pixels that include ACA and MCA branches overestimate CBF. On the other hand, because the partition coefficient of stable xenon in blood and cerebral cells is not so different, this phenomenon does not occur in stable xenon CT studies. Despite CBF overestimation in pixels that included ACA and MCA branches, perfusion CT studies never failed to clearly identify pathologically abnormal cerebral regions, whatever their nature, with slopes close to unity in linear regression analysis. This accurate correlation in cerebral areas with usually lowered blood flow confers adequate reliability on perfusion CT studies in the evaluation of ischemic cerebral parenchyma.

No significant difference was observed between the two software analyses, at least in healthy cerebral regions without ACA and MCA branches and in pathologically abnormal cerebral regions. We thus conclude that both deconvolution methods, the SVD method and the LMS method, are equivalent for this task. In healthy cerebral regions with ACA and MCA branches, the LMS software led to CBF values that were significantly higher than the CBF values obtained using the SVD method. This is because of different arterial detection thresholds and spatial filtering for the final display rather than the deconvolution technique.

Perfusion CT studies were performed at 80 kVp rather than 120 kVp, allowing for a statistically significant increase in contrast enhancement. This results from the more important perfusion of gray matter compared with that of white matter. Moreover, after contrast enhancement, radiographic interaction with soft tissues at 80 kVp relates to the photoelectric effect, due to the 33 keV K-edge of the iodine included in the contrast material. On the other hand, radiographic interaction before contrast material administration is mainly due to the Compton effect (42). Although the use of 80 kVp involves a lower photon flux, it does not result in a statistically significant increase in noise, allowing 80 kVp images to be used in perfusion CT analysis (42). Finally, performance of perfusion CT examination at 80 kVp, keeping milliamperes constant, lowers the radiation dose by a factor of 2.8 (42).

The acquisition of cerebral CT sections every 2 s was justified by the absence of the cine mode on our CT unit at the time of the study. Data acquisition every 2 s rather than every second decreases the radiation dose in half and leads to final perfu-

sion CT CBF values comparable with stable xenon CT results.

An injection rate of 5 cc/s was used for The IV administration of iodinated contrast material. This injection rate was considered as the highest tolerable rate for our patients, although some authors, who use the maximal slope model rather than the central volume principle, have reported the use of injection rates as high as 20 cc/s (43). Although the use of injection rates higher than 5 to 10 cc/s apparently do not induce significant changes in the time-concentration curves in the pulmonary veins and in the aorta, and thus in cerebral arteries (44, 45), the accurate correlation of our results with those of stable xenon CT studies testifies the validity of our choice of a lower injection rate.

The choice of the reference artery for the deconvolution process was an important concern. In one of our cases, it strongly influenced the final CBF map (Fig 4). In this patient, a giant carotid artery altered blood hemodynamics with, as a result, a delayed time-concentration curve in the left MCA. If the reference arterial pixel was chosen upstream from the aneurysm or in the ACA or contralateral MCA, mean transit time and CBF values in the left hemisphere were found falsely high and low, respectively, compared with the stable xenon CBF map. Correct left CBF values were obtained when left hemisphere parenchymal contrast enhancement curves were deconvoluted by the left MCA profile obtained downward of the aneurysm.

In patients with Moya networks, these networks could not be used as reference arteries. In the other patients, the contrast enhancement curves were similar in both ACA and MCA, and the final perfusion CT CBF maps did not vary according to the chosen reference artery. The choice of the reference artery in case of acute strokes, with an occluded cerebral artery, remains to be defined by dedicated studies.

With stable xenon CT, there is no concern regarding the choice of a reference artery, because the arterial time-concentration curve is assumed to be the same as that measured in the end-tidal breathed air. However, this leads to other pitfalls, notably for patients with chronic respiratory disease or with cardiac or vascular shunts.

## Conclusion

In conclusion, we have shown a good correlation between perfusion CT studies of CBF and stable xenon CT results. Perfusion CT values of CBF

←

D, Image obtained using the LMS method. Healthy cerebral regions without ACA and MCA branches show linear regression with strong correlation and slopes close to unity.

E, Image obtained using the LMS method. In healthy cerebral regions with ACA and MCA branches, perfusion CT values of CBF tend to exceed stable xenon CT values.

F, Image obtained using the LMS method. Pathologically abnormal cerebral regions show linear regression with strong correlation and slopes close to unity.



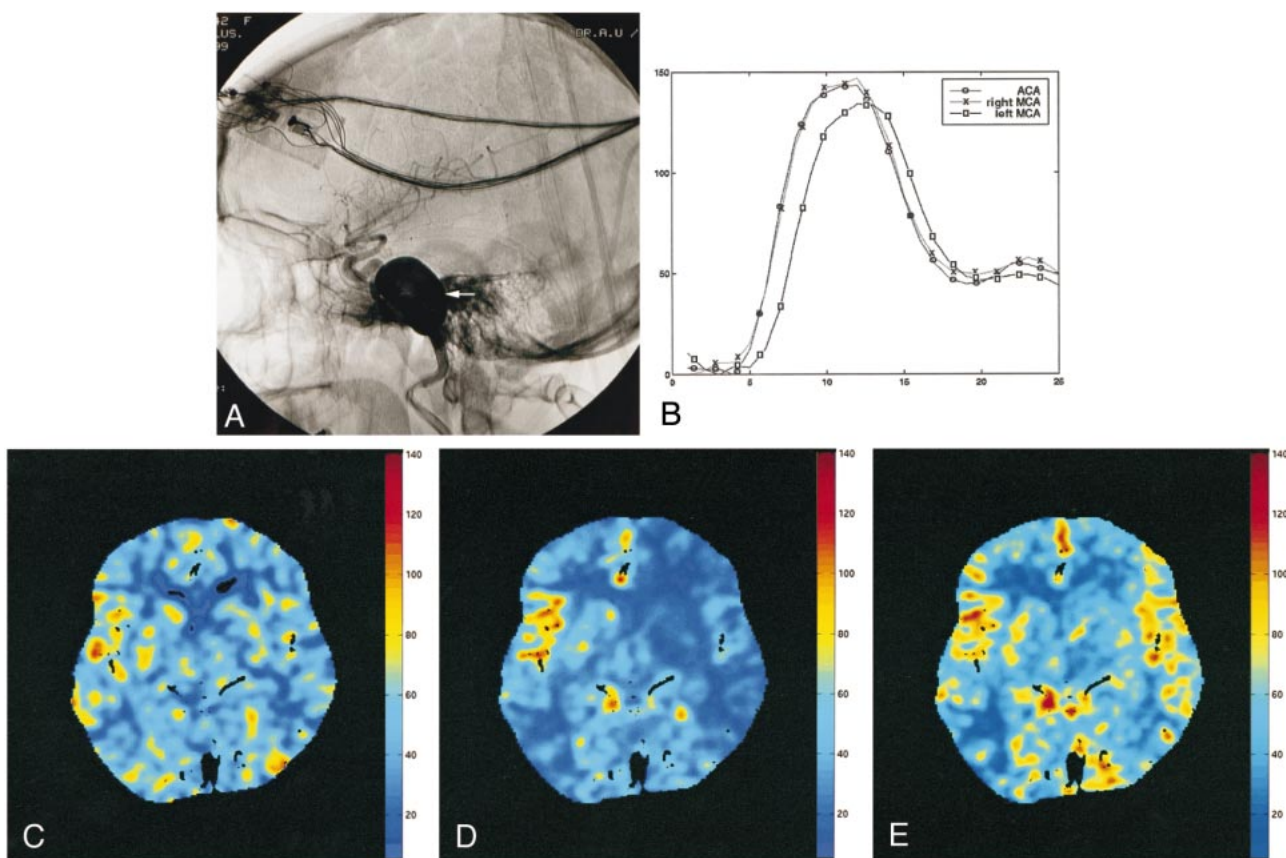


FIG 4. Images from the case of a 57-year-old woman with a diplopia while looking leftward.

A, Lateral angiographic view shows a left giant internal carotid artery aneurysm (arrow) at the C5 segment between the carotid siphon and the intrapetrous carotid artery. Diplopia related to compression of the left VIth cranial nerve by this aneurysm.

B, Analysis of the time-concentration curves in the ACA (circles) and in both MCA (crosses and squares) shows a cerebral flow alteration at the beginning of the left MCA (squares), downward of the aneurysm, featuring a delayed time-to-peak within this artery.

C, Stable xenon CT values of CBF.

D, Choice of the ACA as the reference artery results in a CBF map (cc/[100 g  $\times$  min]) with underestimated CBF on the left side, compared with the stable xenon CT values of CBF.

E, Deconvolution of parenchymal time-concentration curves of each cerebral hemisphere by related profiles in ipsilateral MCA avoids such a pitfall.

were obtained according to the central volume principle, with the application of two non-parametric deconvolution methods, the SVD method and the LMS method, which were shown to be equivalent. The choice of the reference artery for the deconvolution process is a key point that remains to be defined by dedicated studies of cases of acute stroke with occluded cerebral arteries. Perfusion CT studies of CBF thus constitute an accurate and easy-to-perform imaging technique to assess brain perfusion. These studies may become more important and widespread in the management of cases of acute stroke or cases with other CBF alterations. However, further verification for these patients with intracranial arterial occlusion is necessary.

## Appendix

### Deconvolution Methods

Both SVD and the conventional LMS methods basically intend to solve the overdetermined set of

equations corresponding to the algebraic formulation of the deconvolution of parenchymal time-concentration curves by a reference arterial curve. Using the short-hand matrix notation, the related convolution can be expressed by the matrix equation:

$$A \cdot h = p \quad (7)$$

where  $p$  relates to the parenchymal time-concentration curve,  $A$  to the rectangular matrix of shifted versions of the reference arterial curve, and  $h$  to the impulse function in the considered point (46, 47). The CT perfusion software uses SVD for the resolution of this equation, whereas our software, which will soon be available as freeware on our web site (<http://www.hospvd.ch/public/chuv/rad/home.htm>), uses a stable variation of the conventional LMS method.

In the LMS method, the effective rank,  $K$ , of the matrix  $A$  is determined from the QR decomposition with pivoting. The solution  $h$ , which has the most  $K$  non-zero components, is then computed. This method is known to be numerically more stable

than the direct resolution of normal equations of the linear least square problem.

On the other hand, the SVD method builds up matrices  $U$ ,  $W$ , and  $V^T$ , so that if the matrix  $A$  is  $M \times N$ , it can be written as follows:

$$A = U \cdot W \cdot V^T \quad (8)$$

in which  $U$  is an  $M \times N$  column-orthogonal matrix,  $W = [\text{diag}(w_i)]$  is an  $N \times N$  diagonal matrix with positive or zero elements (the singular values  $w_i$  of the system), and  $V^T$  is the transpose of an  $N \times N$  orthogonal matrix. With this decomposition, the solution  $h$  can be found as follows:

$$h = V \cdot \left[ \text{diag} \left( \frac{1}{w_i} \right) \right] \cdot (U^T \cdot p) \quad (9)$$

The SVD method provides a good analysis of the problem: singular values that are zero or close to zero relate to equations that are close to being linear combinations of each other. In terms of sampling data from bolus passage experiments, this means that data are being sampled at time points at which changes in arterial or parenchymal time-concentration curves over time are small with regard to noise. By eliminating diagonal elements below a certain threshold in  $W$ , the effects of noise before calculating  $h$  are consequently minimized. The SVD method is known to be very stable and efficient (46) but suffers from the arbitrary selection of the threshold for elimination of small singular values (47).

### Radiation Dose

The radiation dose for perfusion CT involving 25 successive CT sections obtained on an axial mode at 80 kVp and 200 mAs was evaluated through experimental studies on a test phantom in conformity with the Food and Drug Administration rules, related to a polymethylmethacrylate cylinder, 16 cm in diameter (Code of Federal Regulations, 21 CFR Ch. 1, §1020.3, Food and Drug Administration, Washington, DC, 1992). Calculation of normalized and weighted CT dose index and cerebral effective dose was conducted according to European Guidelines on Quality Criteria for Computed Tomography (48), which are very close to those recommended by the Food and Drug Administration. The brain-absorbed dose was deduced from the normalized and weighted CT dose index (49).

Considering acquisition of two adjacent 10-mm sections, which was available thanks to the multi-detector-array technology, the measured normalized and weighted CT dose index 80 kVp is 0.090 mGy/mAs. Supposing a perfusion CT protocol of 25 successive sections obtained on an axial mode at 200 mAs and with regard to the geometry of radiation delivery on the Lightspeed CT Unit (dose efficiency of 65%), the resultant radiation dose is 291 mGy. Regarding the stochastic effect of radiations, these calculated doses must be redistributed on the

whole cerebral volume. Because a 20-mm thickness relates approximately to one-tenth of the cerebral volume, the brain absorbed dose at 80 kVp is 29 mGy. Considering a weighting factor of 0.0021 mSv/(mGy  $\times$  cm) for the brain, the cerebral effective dose is 1.218 mSv, which is inferior to the reference dose level for a standard cerebral CT examination (2.5 mSv) (48).

### References

1. Reivich M. **Blood flow metabolism couple in brain.** *Res Publ Assoc Res Nerv Ment Dis* 1974;53:125-140
2. Lassen NA. **Cerebral blood flow and oxygen consumption in man.** *Physiol Rev* 1959;39:183-238
3. Harper AM. **Autoregulation of cerebral blood flow: influence of the arterial blood pressure on the blood flow through the cerebral cortex.** *J Neurol Neurosurg Psychiatry* 1966;29:398-403
4. Wood JH. **Cerebral Blood Flow: Physiologic and Clinical Aspects.** New York: McGraw-Hill;1987
5. National Institute of Neurological Disorders and Stroke (NINDS) rt-PA Stroke Study Group. **Tissue plasminogen activator for acute ischaemic stroke.** *N Engl J Med* 1995;33:1581-1587
6. Astrup J, Siesjö BK, Symon L. **Thresholds in cerebral ischemia: the ischemic penumbra.** *Stroke* 1981;12:723-725
7. Hossmann KA. **Neuronal survival and revival during and after cerebral ischemia.** *Am J Emerg Med* 1983;1:191-197
8. Hossmann KA. **Viability thresholds and the penumbra of focal ischemia.** *Ann Neurol* 1994;36:557-565
9. Hacke W, Kaste M, Fieschi C, et al. **Randomised double-blind trial placebo-controlled trial of thrombolytic therapy with intravenous alteplase in acute ischaemic stroke (ECASS II).** *Lancet* 1998;352:1245-1251
10. Hennerici M. **Improving the outcome of acute stroke management.** *Hosp Med* 1999;60:44-49
11. Sorensen AG, Copen WA, Ostergaard L, et al. **Hyperacute stroke: simultaneous measurement of relative cerebral blood volume, relative cerebral blood flow, and mean tissue transit time.** *Radiology* 1999;210:519-527
12. Ezura M, Takahashi A, Yoshimoto T. **Evaluation of regional cerebral blood flow using single photon emission tomography for the selection of patients for local fibrinolytic therapy of acute cerebral embolism.** *Neurosurg Rev* 1996;19:231-236
13. Kety SS. **The theory and applications of the exchange of inert gas at the lungs and tissues.** *Pharmacol Rev* 1951;3:1-41
14. Jacques AA. **Compartmental Analysis in Biology and Medicine.** 2nd ed. Ann Arbor: The University of Michigan Press;1985
15. Winkler SS, Spira J. **Radiopacity of xenon under hyperbaric conditions.** *Am J Roentgenol Radium Ther Nucl Med* 1966;96:1035-1040
16. Gur D, Herron JM, Molter BS, et al. **Simultaneous mass spectrometry and thermoconductivity measurements of end-tidal xenon concentrations: a comparison.** *Med Phys* 1984;11:209-212
17. Winkler SS, Sackett JF, Holden JE, et al. **Xenon inhalation as an adjunct to computerized tomography of the brain: preliminary study.** *Invest Radiol* 1977;12:15-18
18. Kelcz F, Hilal SK, Hartwell P, Joseph PM. **Computed tomographic measurement of the xenon brain-blood partition coefficient and implications for regional cerebral blood flow: a preliminary report.** *Radiology* 1978;127:385-392
19. Drayer BP, Wolfson SK, Reinmuth OM, Dujovny M, Boehnke M, Cook EE. **Xenon enhanced CT for analysis of cerebral integrity, perfusion, and blood flow.** *Stroke* 1978;9:123-130
20. Yonas H, Darby JM, Marks EC, Durham SR, Maxwell C. **CBF measured by Xe-CT: approach to analysis and normal values.** *J Cereb Blood Flow Metab* 1991;17:716-725
21. Fatouros PP, Wist AO, Kishore PR, et al. **Xenon/computed tomography cerebral blood flow measurements: methods and accuracy.** *Invest Radiol* 1987;22:705-712
22. DeWitt DS, Fatouros PP, Wist AO, et al. **Stable xenon versus radiolabeled microsphere cerebral blood flow measurements in baboons.** *Stroke* 1989;20:1716-1723
23. Gur D, Yonas H, Jackson DL, et al. **Simultaneous measurements of cerebral blood flow by the xenon/CT method and the microsphere method: a comparison.** *Invest Radiol* 1985;20:672-677

24. Latchaw RE, Yonas H, Pentheny SL, Gur D. **Adverse reactions to xenon-enhanced CT cerebral blood flow determination.** *Radiology* 1987;163:251-254
25. Meier P, Zierler KL. **On the theory of the indicator-dilution method for measurement of blood flow and volume.** *J Appl Physiol* 1954;12:731-744
26. Zierler KL. **Theoretical basis of indicator-dilution methods for measuring flow and volume.** *Circ Res* 1962;10:393-407
27. Zierler KL. **Equations for measuring blood flow by external monitoring of radioisotopes.** *Circ Res* 1965;16:309-321
28. Axel L. **Tissue mean transit time from dynamic computed tomography by a simple deconvolution technique.** *Invest Radiol* 1983;18:94-99
29. Axel L. **Cerebral blood flow determination by rapid-sequence computed tomography: theoretical analysis.** *Radiology* 1980;137:679-686
30. Axel L. **A method of calculating brain blood flow with a CT dynamic scanner.** *Adv Neurol* 1981;30:67-71
31. Wintermark M, Maeder P, Thiran J, Schnyder P, Meuli R. **Quantitative assessment of regional cerebral blood flows by perfusion CT studies at low injection rates: a critical review of the underlying theoretical models.** *Eur Radiol* (in press)
32. Ladurner G, Zilkha E, Iliff LD, du Boulay GH, Marshall J. **Measurement of regional cerebral blood volume by computerized axial tomography.** *J Neurol Neurosurg Psychiatry* 1976;39:152-158
33. Zilkha E, Ladurner G, Iliff LD, Du Boulay GH, Marshall J. **Computer subtraction in regional cerebral blood-volume measurements using the EMI-scanner.** *Br J Radiol* 1976;49:330-334
34. Ladurner G, Zilkha E, Sager WD, Iliff LD, Lechner H, Du Boulay GH. **Measurement of regional cerebral blood volume using the EMI 1010 scanner.** *Br J Radiol* 1979;52:371-374
35. Larson OA, Lassen NA. **Cerebral hematocrit in normal man.** *J Appl Physiol* 1964;19:571-574
36. Sakai F, Nakazawa K, Tazaki Y, et al. **Regional cerebral blood volume and hematocrit measured in normal human volunteers by single-photon emission tomography.** *J Cereb Blood Flow Metab* 1985;5:207-213
37. Nabavi DG, Cenic A, Craen RA, et al. **CT assessment of cerebral perfusion: experimental validation and initial clinical experience.** *Radiology* 1999;213:141-149
38. Cenic A, Nabavi DG, Craen RA, Gelb AW, Lee TY. **Dynamic CT measurement of cerebral blood flow: a validation study.** *AJNR Am J Neuroradiol* 1999;20:63-73
39. Nabavi DG, Cenic A, Dool J, et al. **Quantitative assessment of cerebral hemodynamics using CT: stability, accuracy, and precision studies in dogs.** *J Comput Assist Tomogr* 1999;23:506-515
40. Muizelaar JP, Fatouros PP, Schroder ML. **A new method for quantitative regional cerebral blood volume measurements using computed tomography.** *Stroke* 1997;28:1998-2005
41. Doerfler A, Engelhorn T, von Kummer R, et al. **Are iodinated contrast agents detrimental in acute cerebral ischemia? an experimental study in rats.** *Radiology* 1998;206:211-217
42. Wintermark M, Maeder P, Verdun FR, et al. **Using 80 kVp versus 120 kVp in perfusion CT measurement of regional cerebral blood flow.** *AJNR Am J Neuroradiol* 2000;21:1881-1884
43. Koenig M, Klotz E, Luka B, Venderink DJ, Spittler JF, Heuser L. **Perfusion CT of the brain: diagnostic approach for early detection of ischemic stroke.** *Radiology* 1998;209:85-93
44. Claussen CD, Banzer D, Pfretzschner C, Kalender WA, Schorner W. **Bolus geometry and dynamics after intravenous contrast medium injection.** *Radiology* 1984;153:365-368
45. Reiser UJ. **Study of bolus geometry after intravenous contrast medium injection: dynamic and quantitative measurements (Chronogram) using an X-ray CT device.** *J Comput Assist Tomogr* 1984;8:251-262
46. Ostergaard L, Weisskoff RM, Chesler DA, et al. **High resolution measurement of cerebral blood flow using intravascular tracer bolus passages: part I. mathematical approach and statistical analysis.** *Magn Reson Med* 1996;36:715-725
47. Liu HL, Pu Y, Liu Y, et al. **Cerebral blood flow measurement by dynamic contrast MRI using singular value decomposition with an adaptive threshold.** *Magn Reson Med* 1999;42:167-172
48. European Guidelines on Quality Criteria for Computed Tomography, EUR 16262 EN, 1999. Available at: <http://www.dr.dk/guidelines/ct/quality/>. Accessed
49. Hidajat N, Mäurer J, Schröder RJ, et al. **Relationships between physical dose quantities and patient dose in CT.** *Br J Radiol* 1999;72:556-561